



Artefacts at different distances from titanium and zirconia implants in cone-beam computed tomography: effect of tube current and metal artefact reduction

Arthur Xavier Maseti Mancini¹ · Matheus Urias Cruz Santos² · Hugo Gaêta-Araujo³ · Camila Tirapelli⁴ · Ruben Pauwels⁵ · Christiano Oliveira-Santos⁶

Received: 22 July 2020 / Accepted: 29 January 2021 / Published online: 5 February 2021
© The Author(s), under exclusive licence to Springer-Verlag GmbH, DE part of Springer Nature 2021

Abstract

Objectives To evaluate the effect of cone-beam computed tomography (CBCT) tube current (mA) on the magnitude of artefacts at different distances from titanium or zirconia implants, with and without activation of a proprietary metal artefact reduction (MAR).

Material and methods Human mandibles were scanned on an OP300 Maxio CBCT unit (Instrumentarium, Tuusula, Finland) before and after the installation of dental implants, with four different tube currents (4 mA, 6.3 mA, 8 mA and 10 mA), with and without activation of proprietary MAR. The effect of mA on the standard deviation (SD) of gray values and contrast to noise ratio (CNR) were assessed in regions of interest located 1.5 cm, 2.5 cm, and 3.5 cm from implants.

Results In the presence of titanium implants, a significant decrease in SD was found by increasing tube current from 4 mA to 6.3 mA or 8 mA. For zirconia implants, 8 mA yielded better results for all distances. MAR improved CNR in the presence of zirconia implants at all distances, whereas no differences were observed with the use of MAR for titanium implants.

Conclusion Increased tube current can improve overall image quality in the presence of implants, at all the distances tested. When a zirconia implant is present, such increase in mA should be higher in comparison to that for examinations with titanium implants. Activation of OP300 Maxio proprietary MAR improved image quality only among examinations with zirconia implants.

Clinical relevance Artefact-generating implants are common in the field of view of CBCT examinations. Optimal exposure parameters, such as tube current, ensure high image quality with lowest possible radiation exposure.

Keywords Cone-beam computed tomography · Artefacts · Titanium implants · Zirconia implants · Tube current

Introduction

The presence of high density and high atomic number materials (e.g., metals) in the field of view (FOV) of cone-beam

computed tomography (CBCT) examinations may generate a considerable amount of image artefacts [1–3]. Artefacts are discrepancies between the visualized structure and the real content of the object under investigation [1, 2], decreasing

✉ Arthur Xavier Maseti Mancini
arthur.mancini@usp.br

¹ Department of Dental Materials and Prosthodontics, School of Dentistry of Ribeirao Preto, University of Sao Paulo, Av. Do Café, s/n, Ribeirao Preto, Sao Paulo 14040-904, Brazil

² Department of Stomatology, Public Oral Health and Forensic Dentistry, Division of Oral Radiology, School of Dentistry of Ribeirao Preto, University of Sao Paulo, Av. Do Café, s/n, Ribeirao Preto, Sao Paulo 14040-904, Brazil

³ Department of Oral Diagnosis, Division of Oral Radiology, Piracicaba Dental School, University of Campinas, Av. Limeira, 901, Piracicaba, São Paulo 13414-903, Brazil

⁴ Department of Dental Materials and Prosthodontics, School of Dentistry of Ribeirao Preto, University of Sao Paulo, Av. Do Café, s/n, Ribeirao Preto, Sao Paulo 14040-904, Brazil

⁵ Medical Physics & Quality Assessment, Department of Imaging & Pathology, Catholic University of Leuven, Leuven, Belgium and Aarhus Institute of Advanced Studies, Aarhus University, Høegh-Guldbergs Gade 6B, 8000 Aarhus, Denmark

⁶ Department of Stomatology, Public Oral Health and Forensic Dentistry, Division of Oral Radiology, School of Dentistry of Ribeirao Preto, University of Sao Paulo, Av. Do Café, s/n, Ribeirao Preto, Sao Paulo 14040-904, Brazil

the diagnostic quality of images [2]. Artefacts are more pronounced in the vicinity of the metal; however, they can extend for at least 3.5 cm around implants [4].

Due to the high atomic number of implant materials, the most common types of artefact are due to beam hardening and photon starvation. Beam hardening occurs because the object acts as a filter that predominately blocks X-ray photons with less energy. The resulting discrepancy in average energy between different areas of the detector manifests as errors in the reconstruction of the data, which are visualized as linear structures, shadows, and organized bands [5]. Similarly, photon starvation causes errors in the projection data due to (almost) complete attenuation of the X-ray beam by large and/or dense metal objects. When these effects are combined with other effects such as X-ray scatter noise, they generate a significant variation in gray values close to very dense materials, producing images that can be diagnostically unacceptable, since artefacts can obscure nearby structures and pathoses [6].

CBCT uses higher radiation doses compared with other dental imaging exams, such as periapical and panoramic radiographs. The ALADA principle (as low as diagnostically acceptable) should be applied to all examinations that use ionizing radiation, in order to balance the image quality and the radiation dose for acceptable diagnostic results [7]. The optimization of CBCT images can be performed by selecting appropriate acquisition protocols for specific diagnostic tasks. Field of view (FOV), voxel size, scan time, half/full rotation, tube voltage (kV), and tube current (mA) are examples of scan settings that can be adjusted for optimized application of CBCT [8–10]. Furthermore, several CBCT systems have implemented reconstruction algorithms for metal artifact reduction (MAR). MAR is an umbrella term that covers a variety of algorithms. There are different ways to categorize MAR techniques, e.g., projection-domain methods vs. image-domain methods vs. hybrid methods [11]. Whereas the exact operation of these MAR algorithms is not disclosed by manufacturers, it can be stipulated that current MAR implementations in CBCT are based on the projection completion method [11], in which missing values are interpolated from neighboring pixels. Although more complex MAR algorithms have been described in literature [11], e.g., through physical modeling of the X-ray spectrum or mathematical modeling of the artefact pattern, their implementation in clinical practice is typically hampered by the excessive reconstruction time. The potential of MAR in CBCT to improve diagnosis is controversial; however, currently implemented MAR techniques seem to decrease standard deviation of gray values (SD) and increase contrast-to-noise ratio (CNR) in the vicinity of structures with high density and/or high atomic number [12–15].

Higher mA, in general, improves image quality by reducing noise. However, there is a direct proportional relationship between mA and the radiation dose to the patient [16]. Therefore, the evaluation of the effect of variations in mA

for specific diagnostic tasks is relevant to the optimized use of the CBCT. A recent study showed that the increase in mA significantly improves the diagnostic performance in detecting vertical root fractures in teeth with metal posts and gutta-percha [17]. On the other hand, the use of lower mA, despite its effect on image quality (i.e., greater noise), can significantly reduce the radiation dose employed and still produce clinically acceptable results for specific diagnostic tasks [16, 17]. Therefore, further studies are needed to improve the recommendations of specific protocols for CBCT exams, both for the purpose of evaluating implants and for other indications when implants are present in the FOV.

The objective of this study was to evaluate the effect of CBCT tube current (mA) on the magnitude of the artefacts caused by titanium and zirconia implants at different distances from the artefact-generating object, with and without activation of a proprietary metal artefact reduction (MAR) tool, by measuring SD and CNR in selected regions of interest of the images.

Methodology

Sample preparation

Cylindrical phantoms, containing human mandibles immersed in ballistic gelatin [18], were created for this study. Ten eviscerated human mandibles were obtained from the Anatomy Laboratory of Ribeirão Preto School of Dentistry. The mandibles were placed in the center of a cylindrical plastic box (16-cm diameter) containing 1 cm in height of ballistic gelatin, previously poured into the container. A $1.8 \times 1.0 \times 0.7$ cm block of dental impression material (Condensation Silicone - Yller Reflex, Pelotas, Brazil) was placed on the buccal cortex of the anterior region of each mandible, at the center of the alveolar ridge. Two cervical vertebrae (C1 and C2) were placed posterior to the mandibles, and ballistic gelatin was then poured into the boxes to form 16 x 8cm cylindrical phantoms (Fig. 1).

CBCT image acquisition

For the acquisition of CBCT images, an acrylic device with 16-cm diameter (Fig. 1a) was manufactured to attach to the support of the machine and allow the standardized positioning of the phantoms and location of the FOV. The phantoms were then scanned using an OP300 Maxio CBCT unit (Instrumentarium, Tuusula, Finland), operating at 90 kV, 0.085 mm voxel size, 8×6 cm FOV. The tube current was set at four different levels: 4 mA, 6.3 mA, 8 mA and 10 mA. The metal artefact reduction (MAR) tool was disabled during the acquisition of the exams. After each acquisition without

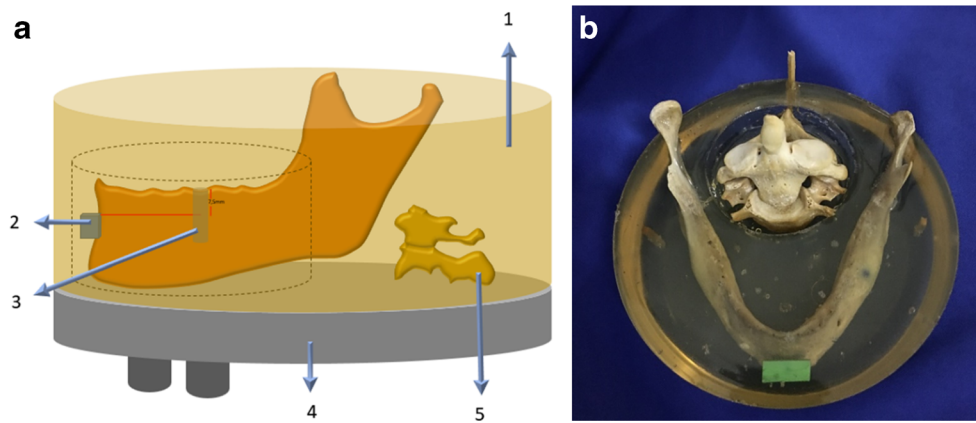


Fig. 1 Schematic drawing (a) and photograph (b) showing lateral and upper views, respectively, of the ballistic gelatin phantom containing the mandible and cervical vertebrae, supported by the standardized device for the acquisition of tomographic images. 1, Ballistic gelatin; 2,

condensation silicone block; 3, Implant to be installed in the region of tooth 46; 4, Acrylic device produced to standardize acquisitions; 5, Cervical vertebrae. The cylinder with dotted lines represent the field of view in the CBCT exams (8x6cm)

MAR, new reconstructions of the same raw data were obtained with the activation of MAR algorithms.

After the acquisition of the initial images (i.e., mandibles without implants), 3.75×13 mm titanium implants (HE Conico - Intraoss, São Paulo - Brazil) were installed in 5 mandibles, and 3.3×12 mm zirconia implants (Pure Ceramic - Straumann, Basel - Switzerland) in the other 5 mandibles. All implants were inserted in the edentulous region corresponding to tooth 46. The portion of the ballistic gelatin covering the region was removed, an osteotomy following a sequence of drills recommended by the manufacturers was performed, and the implant was inserted manually using a ratchet. After implant placement, new gelatin was poured to refill the removed portions.

The phantoms with the implants were then scanned using the same scanning parameters described above. Therefore, a total of 160 exams were acquired (10 phantoms x before/after implant placement x 4 different tube currents x with/ without MAR—Fig. 2). Axial slices were exported in DICOM format for analysis using ImageJ (National Institutes of Health, Bethesda, MD, USA) based on the study of Fontenele et al. (2018).

Image assessment

Regions of interest (ROI) in the homogeneous regions (i.e., ballistic gelatin) were selected at the level of the implants to assess the effect of tube current on artefacts, which occur along the direction of the x-ray projection. In the axial slice in which the condensation silicone block was first visualized, a line was determined in the center of the implant and following the long axis of the mandibular body on the right side. Additional lines were then determined at different angles from the first line (65°, 90°, 115°, and 140°). From the center of the implant, three semicircles with radii of 1.5, 2.5, and 3.5 cm were drawn. Finally, twelve 2.8×2.8 mm regions of interest

(ROI) were established at the intersection of the circles and lines (Fig. 3). Mean (M) and the standard deviation (SD) of the gray values were registered for each ROI. The macro-function of ImageJ was used to determine and evaluate the same ROIs of each phantom in different conditions. An additional ROI was determined in the condensation silicone block to serve as a control area for the calculation of the contrast-to-noise ratio (CNR) according to the formula below [12]. Lower SD and higher CNR are associated with better image quality.

$$CNR = \frac{M_{IMPLANT} - M_{CONTROL}}{\sqrt{SD_{IMPLANT}^2 + SD_{CONTROL}^2}}$$

Data analysis

Standard deviation (SD) and the contrast-to-noise ratio (CNR) were compared with repeated measures analysis of variance (ANOVA) and post-hoc Tukey’s test in order to test the effects of different tube currents at different distances from titanium and zirconia implants, and the effect of MAR algorithm. Statistical analyses were performed using SPSS software (IBM Corp., Armonk, NY - USA), with significance level set at $\alpha=0.05$.

Results

Mean SD values of the ROIs at different distances from the implants, with and without MAR and with different tube currents, are shown in Table 1. Overall, an increase in mA resulted in significant decrease of SD ($p \leq 0.05$). In the presence of titanium implants, significant decrease in SD was achieved by increasing tube current from 4 mA to 6.3 mA or 8 mA. For the zirconia implants, 8 mA yielded better results for all distances.

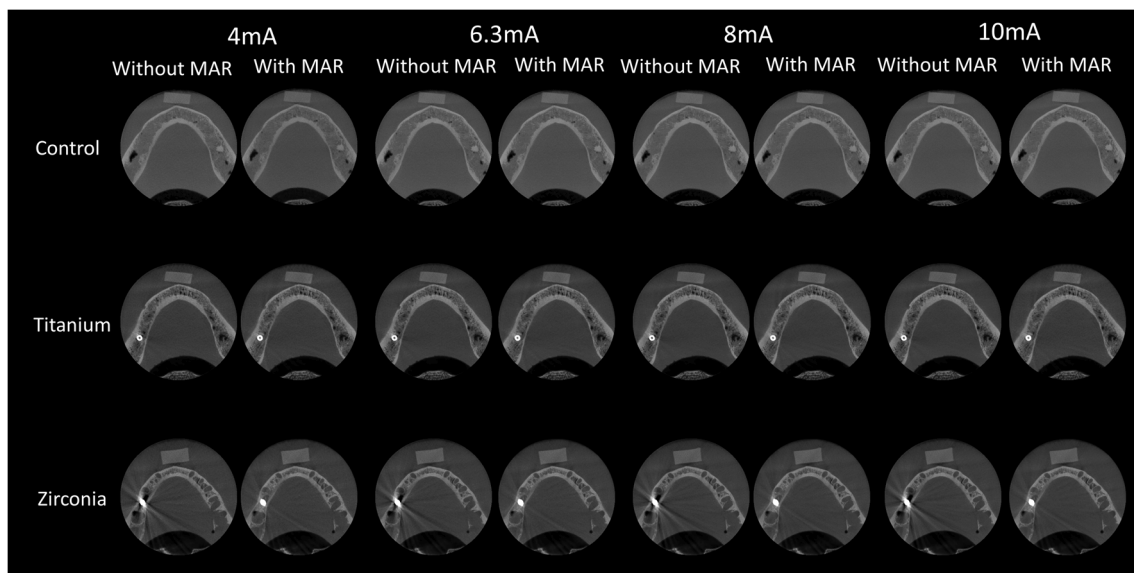


Fig. 2 Axial Images represent implants (control in the first row, titanium in the second row, and zirconia in the third row) with different tube currents (4 mA, 6.3 mA, 8 mA, and 10 mA) and with/without the application of MAR

ROIs at 1.5 cm from zirconia implants had significantly higher SD than those in the titanium implant and control groups. There was no statistically significant difference in SD between ROIs with and without MAR for control and implant groups ($p > 0.05$). However, in the zirconia group, lower SD was achieved by the activation of MAR at 2.5 cm distance for all tube currents and at 3.5 cm for 8 mA ($p \leq 0.05$).

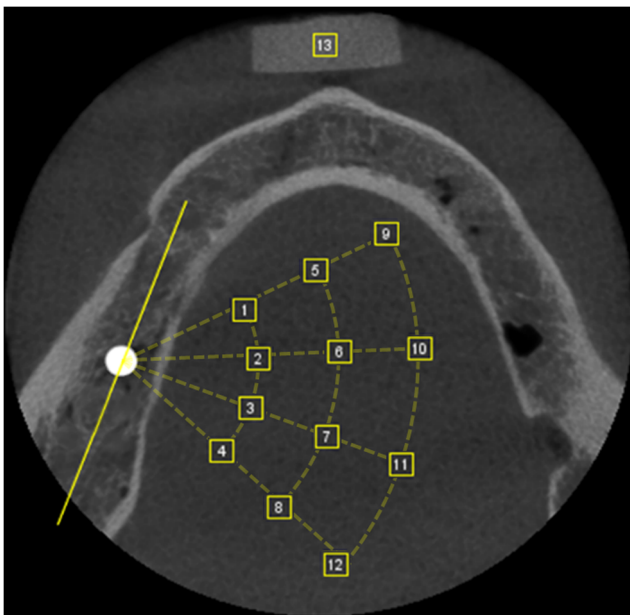


Fig. 3 Regions of interest in the ballistic gel (1–12) and silicone block (13). Initially, a reference line was drawn along the long axis of the hemimandible and passing through the center of the implant. Additional lines were then determined at 65°, 90°, 115°, and 140° (dotted lines) from the reference line. Three semicircles with radii of 1.5, 2.5 and 3.5 cm (dotted curves) were drawn from the center of the implant. Finally, the center of the twelve ROIs was determined at the intersection of the circles and lines (adapted from Fontenele et al., 2018)

Mean CNR values of the ROIs are shown in Table 2, with and without MAR, according to tube currents and distances. In the presence of implants, significant increase in mean CNR at all three distances is observed when tube current is increased from 4 mA to 6.3 mA ($p \leq 0.05$). In all tube currents, lower CNR was observed at 1.5 cm from the zirconia implants compared with the titanium implants, and at 4 mA, the CNR was lower at all distances without MAR ($p \leq 0.05$). There were no significant differences between scans with or without MAR in the control and titanium group, but MAR use increased CNR values in most conditions tested (mA vs distances) in the zirconia group ($p \leq 0.05$).

Discussion

The assessment of the impact of different CBCT parameters on the formation of image artefacts is essential to promote optimized CBCT acquisition protocols, combining the lowest radiation possible with the best image quality achievable for different diagnostic tasks [8, 9, 13, 16, 19–22]. Similar to the results observed in the present study for titanium and zirconia implants, a previous study found that higher mA reduced the magnitude of artefacts related to metallic intracanal posts at different distances from the artefact-generating material [14]. There is a direct relationship between tube current, radiation dose, and image quality [5, 16]. Therefore, practical decisions for optimal tube current applied to CBCT acquisition should take into consideration the image requirements of specific diagnostic tasks [14, 16, 17].

Overall, when tube current increased from 4 mA to 6.3 mA or 8 mA, significantly less artefacts (i.e., higher CNR and lower SD values) were found for both titanium and zirconia

Table 1 Mean SD of gray values of the ROIs from control (no implant), titanium, and zirconia implant groups, according to their distance to the implant, tube current (mA) and MAR condition.

Group	Distance	SD of gray values–mean (standard deviation)							
		Without MAR				With MAR			
		4 mA	6.3 mA	8 mA	10 mA	4 mA	6.3 mA	8 mA	10 mA
Control	1.5 cm	41.9 ^a (7.4)	34.5 ^b (5.8)	33.2 ^b (5.7)	29.6 ^c (1.4)	41.9 ^a (7.4)	34.5 ^b (5.8)	33.2 ^b (5.7)	30.2 ^c (6.0)
	2.5 cm	39.7 ^a (3.2)	32.4 ^b (2.8)	29.6 ^c (2.9)	28.4 ^c (2.5)	39.7 ^a (3.2)	32.4 ^b (2.8)	29.6 ^c (2.9)	28.5 ^c (2.3)
	3.5 cm	38.6 ^a (3.7)	32.9 ^b (3.1)	30.4 ^c (2.6)	28.9 ^d (3.3)	38.3 ^a (3.0)	32.6 ^b (2.8)	30.1 ^c (2.2)	28.9 ^d (2.9)
Titanium	1.5 cm	41.8 ^a (0.9)	34.0 ^b (1.3)	33.4 ^b (1.8)	32.0 ^b (0.6)	41.5 ^a (4.3)	35.0 ^b (3.8)	34.5 ^b (4.6)	33.3 ^b (3.6)
	2.5 cm	41.0 ^a (5.90)	33.9 ^b (6.7)	33.1 ^b (6.20)	31.4 ^b (4.8)	41.0 ^a (5.0)	33.5 ^b (6.5)	33.7 ^b (5.1)	32.0 ^b (4.3)
	3.5 cm	37.20 ^a (1.5)	33.0 ^b (1.5)	29.9 ^c (1.4)	29.0 ^c (2.2)	37.7 ^a (2.4)	34.0 ^b (2.5)	30.8 ^c (3.1)	30.1 ^c (2.5)
Zirconia	1.5 cm	63.1 ^{a*} (18.3)	57.2 ^{a*} (18.0)	53.5 ^{b*} (18.1)	53.1 ^{b*} (20.9)	55.3 ^{a*} (21.6)	49.7 ^{a*} (21.6)	47.4 ^{b*} (21.3)	46.6 ^{b*} (22.2)
	2.5 cm	42.5 ^a (6.4)	36.0 ^b (3.9)	33.4 ^{bc} (5.3)	32.8 ^c (5.2)	38.7 ^{a†} (4.8)	32.2 ^{b†} (2.9)	30.9 ^{b†} (4.9)	29.1 ^{b†} (4.1)
	3.5 cm	40.3 ^a (4.2)	35.9 ^a (3.5)	33.3 ^{ab} (3.20)	30.5 ^b (1.2)	38.6 ^a (4.3)	33.7 ^b (2.9)	31.2 ^{b†} (3.8)	28.9 ^b (1.6)

^{a,b,c,d} Different superscript letters within each row indicate statistically significant differences ($p \leq 0.05$) between tube currents (mA), with “a” indicating the highest SD value in the row (i.e. worst image quality)

groups, at all three distances from implants. The analysis of the SD of gray values and the CNR has been widely used in previous studies to demonstrate the magnitude and extension of artefacts at different distances [5, 12, 23, 24]. High SD and low CNR values are associated with degradation of the image, which is usually higher in the vicinity of the implants [3–5, 23]. Artefacts are reduced at increasing distances to the metal object in the axial plane due to the fact that the number of projections in which the metal overlaps with a given ROI is inversely proportional to the distance between the metal and the ROI. In other words, an area that is at a longer distance to a metal object is reconstructed using a higher number of non-compromised projections, resulting in reduced artefact severity. Of course, in the presence of multiple metal objects, more complex artefact patterns will occur.

In this study, significant differences in SD and CNR were observed between zirconia and control groups in ROIs located at 1.5 cm distance from implants, even when the tube current was increased. At 2.5 cm from the zirconia implant, an increase in mA improved CNR, and the difference to the controls became non-significant at that distance. Similarly, at 1.5 cm from titanium implants, CNR increased to values comparable to control when tube current was increased from 4 mA to 6.3 mA. When MAR was activated, CNR significantly increased for the ROIs in the zirconia group. However, SD at 1.5 cm from zirconia implants remained significantly

different from the control with MAR. These results show that image degradation within 1.5 cm from zirconium remained high, even with the improved CNR observed at all distances caused by increased mA and MAR activation. Zirconia implants are known to generate more artefacts than titanium implants [3, 19], which is consistent with the difference in their atomic numbers ($Z = 40$ and $Z = 22$, respectively).

The activation of MAR increased CNR at all three distances only for the zirconia group, regardless of the tube current used. Also, a significant decrease in SD related to MAR activation was observed only for all ROIs located at 2.5 cm from zirconia implants, and those at 3.5 cm from zirconia implants with 8 mA. However, no effect of MAR was observed for titanium implants. As MAR has been shown to be effective only when artifacts are pronounced [20, 21], in the control group (i.e., without implants) and in the titanium group the effect of the tool was limited or even non-existent. Importantly, MAR is a tool that acts in the image post-processing step and therefore does not affect the radiation dose, only the reconstruction time [22]. Literature reports that in the presence of implants, the MAR tool does not affect the vicinity of implants [13] and has not improved different diagnostic tasks close to implants [25]. However, there is no consensus on the influence of MAR. It is important to note that, while it can be assumed that commercially implemented MAR algorithms in CBCT are based on the projection completion

Table 2 Mean CNR values of the ROIs from control (no implant), titanium and zirconia implant groups, according to their distance to the implant, tube current (mA) and MAR condition

Group	Distance	CNR–mean (standard deviation)							
		Without MAR				With MAR			
		4 mA	6.3 mA	8 mA	10 mA	4 mA	6.3 mA	8 mA	10 mA
Control	1.5 cm	8.0 ^a (0.9)	9.1 ^b (1.3)	9.5 ^c (1.4)	9.9 ^c (1.7)	8.0 ^a (0.9)	9.1 ^b (1.3)	9.5 ^c (1.4)	9.7 ^c (1.5)
	2.5 cm	8.3 ^a (1.5)	9.5 ^b (2.0)	10.1 ^c (2.3)	10.3 ^c (2.4)	8.3 ^a (1.5)	9.5 ^b (2.0)	10.1 ^c (2.3)	10.2 ^c (2.3)
	3.5 cm	8.3 ^a (1.5)	9.4 ^b (1.9)	9.94 ^c (2.2)	10.15 ^c (2.5)	8.3 ^a (1.5)	9.4 ^b (1.9)	9.9 ^c (2.2)	10.0 ^c (2.4)
Titanium	1.5 cm	7.1 ^{a*} (0.7)	8.2 ^b (0.8)	8.4 ^b (1.1)	8.5 ^b (0.8)	7.3 ^a (1.0)	8.1 ^b (1.1)	8.3 ^b (1.3)	8.4 ^b (1.1)
	2.5 cm	7.1 ^a (0.8)	8.1 ^b (0.8)	8.36 ^b (1.3)	8.5 ^b (0.9)	7.1 ^a (1.0)	8.0 ^b (1.1)	8.2 ^b (1.4)	8.3 ^b (1.1)
	3.5 cm	7.3 ^a (1.1)	8.2 ^b (1.1)	8.59 ^b (1.6)	8.7 ^b (1.3)	7.3 ^a (1.3)	8.0 ^b (1.3)	8.4 ^b (1.7)	8.5 ^b (1.4)
Zirconia	1.5 cm	6.8 ^{a*} (1.3)	7.7 ^{b*} (1.5)	8.1 ^{b*} (1.8)	7.8 ^{b*} (1.8)	7.7 ^{a†} (1.2)	8.7 ^{b†} (1.4)	9.0 ^{c†} (1.3)	8.8 ^{c†} (1.4)
	2.5 cm	8.5 ^{a*} (2.0)	9.7 ^b (2.1)	10.3 ^b (2.5)	9.8 ^b (2.4)	9.0 ^{a†} (1.9)	10.3 ^{b†} (2.0)	10.8 ^{c†} (2.6)	10.4 ^{c†} (2.4)
	3.5 cm	8.4 ^{a*} (1.7)	9.5 ^b (2.0)	9.9 ^b (2.3)	9.6 ^b (2.0)	8.8 ^{a†} (1.8)	9.9 ^b (2.0)	10.4 ^{c†} (2.3)	10.1 ^{c†} (2.0)

^{a,b,c} Different superscript letters within each row indicate statistically significant differences ($p \leq 0.05$) between tube currents (mA), with “a” indicating the lowest CNR value in the row (i.e., worst image quality)

method, it could be implemented in various ways by different manufacturers, e.g., linear interpolation vs. other types of interpolation, single correction vs. iterative reprojection [11]. Further studies should be carried out to assess the true impact of MAR under different circumstances and in different CBCT units.

In the present study, human mandibles and adjacent vertebrae were included in ballistic gelatin, which has been considered the best material to simulate the attenuation and dispersion caused by soft tissues [18]. The 8 x 6 cm FOV used in this study encompassed only part of the phantom. C1 and C2 vertebrae were added for a more realistic composition of the exomass [26] involved in CBCT examinations of the mandible. An acrylic device was used to guide the position of the standardized phantoms, and scripts and macros from ImageJ software were used for each of the 10 mandibles, to ensure precise assignment of all ROIs in the images with different tube currents, as well as before and after implant placement. ROIs were placed in areas containing ballistic gelatin, which would correspond to the location of soft tissues in a clinical scenario. The aim of the study was not to assess the influence of artefacts on soft tissue; however, the selection of a homogeneous material was important to compare the influence of the different tube current settings on image quality parameters measured at different distances from the implants.

There are limitations in all studies that use SD and CNR to quantify the formation of artefacts. One limitation is related to the concomitant influence of noise inherent to CBCT images, which affects mainly SD (and therefore CNR) values. In other words, it is impossible to determine how much the effects on SD and CNR in this study are due to reduced quantum noise rather than artefact reduction. Another limitation is related to the fact that the streaks generated by high atomic number materials have a variable spacing pattern. Therefore, ROIs may be completely or partially included in these streaks in some of the mandibles. This justifies the importance of analyzing multiple ROIs in different mandibles with varying anatomical configurations, and it explains the relatively high variance of the CNR and SD values, particularly among the ROIs near zirconia implants.

The results of this study showed that noise and artefacts related to the presence of implants may be reduced by an increase in tube current. For the conditions studied, 6.3 mA yielded the best results for most of the conditions with titanium implants, with or without MAR. For zirconia implants, the best results were found when 8 mA was used with MAR. The influence of tube current on SD and CNR is clear; however, recommendation of specific mA values cannot be determined for all diagnostic tasks, number and distribution of implants, or for multiple CBCT machines [16] due to several

combinations of acquisition parameters employed in each CBCT model. Previous studies have shown, for example, that artefacts produced by implants are influenced by their anatomical location in the dental arch [27] and are more pronounced when implants have peripheral locations in the FOV [28]. Furthermore, FOV size impacts image quality due to the influence of scatter radiation [29]. Voxel size does not seem to affect the production of beam-hardening-related artefacts [19], whilst higher kV is associated with reduced expression of artefacts at different distances from titanium and zirconia implants [20]. Whether or not an increase in radiation dose due to a higher tube current is warranted remains an open question and will need to be addressed for specific diagnostic tasks.

In conclusion, increased tube current can improve overall image quality in the presence of implants, at all the distances tested. The increase in tube current should be higher when a zirconia implant is present, compared with that for examinations with titanium implants. Activation of the proprietary MAR tested (Instrumentarium OP300 Maxio) improved image quality only among examinations with zirconia implants. The effect of MAR should be evaluated for other CBCT models. More evidence regarding potential improvement in image quality and diagnostic performance is needed, especially considering the linear relation between tube current and radiation dose.

Funding Grant #2018/22952-7, São Paulo Research Foundation (FAPESP). This study was financed in part by the Coordenação de Aperfeiçoamento de Pessoal de Nível Superior – Brasil (CAPES) – Finance Code 001. R Pauwels is supported by (1) the European Union Horizon 2020 Research and Innovation Programme under the Marie Skłodowska-Curie grant agreement number 754513 and by Aarhus University Research Foundation (AIAS-COFUND); (2) Internal research fund of Katholieke Universiteit Leuven (grant number C24/18/065). MUC Santos received scholarship from PUB-USP (Programa Unificado de Bolsas – University of São Paulo).

Declarations

Conflict of interest Author AXMM declares that he has no conflict of interest. Author MUCS declares that he has no conflict of interest. Author HGA declares that he has no conflict of interest. Author CT declares that she has no conflict of interest. Author RP declares that he has no conflict of interest. Author COS declares that he has no conflict of interest.

Ethical approval All procedures performed in studies involving human participants were in accordance with the ethical standards of the institutional and/or national research committee and with the 1964 Helsinki declaration and its later amendments or comparable ethical standards.

Informed consent For this type of study, formal consent is not required.

References

- Schulze R, Heil U, Gross D, Bruellmann DD, Dranischnikow E, Schwanecke U, Schoemer E (2011) Artefacts in CBCT: a review. *Dentomaxillofac Radiol* 40:265–273. <https://doi.org/10.1259/dmfr/30642039>
- Nagarajappa AK, Dwivedi N, Tiwari R (2015) Artifacts: The downturn of CBCT image. *J Int Soc Prev Community Dent* 5: 440–445. <https://doi.org/10.4103/2231-0762.170523>
- Sancho-Puchades M, Hämmerle CH, Benic GI (2015) In vitro assessment of artifacts induced by titanium, titanium-zirconium and zirconium dioxide implants in cone-beam computed tomography. *Clin Oral Implants Res* 26:1222–1228. <https://doi.org/10.1111/clr.12438>
- Fontenele RC, Nascimento EH, Vasconcelos TV, Noujeim M, Freitas DQ (2018) Magnitude of cone beam CT image artifacts related to zirconium and titanium implants: impact on image quality. *Dentomaxillofac Radiol* 47:20180021. <https://doi.org/10.1259/dmfr.20180021>
- Pauwels R, Stamatakis H, Bosmans H, Bogaerts R, Jacobs R, Horner K, Tsiklakis, K, SEDENTEXCT Project Consortium (2013) Quantification of metal artifacts on cone beam computed tomography images. *Clin Oral Implants Res* 24(Suppl A100):94–99. <https://doi.org/10.1111/j.1600-0501.2011.02382.x>
- Schulze RK, Berndt D, d'Hoedt B (2010) On cone-beam computed tomography artifacts induced by titanium implants. *Clin Oral Implants Res* 21:100–107. <https://doi.org/10.1111/j.1600-0501.2009.01817.x>
- Carter L, Farman AG, Geist J, Scarfe WC, Angelopoulos C, Nair MK, Hildebolt CF, Tyndall D, Shrout M, American Academy of Oral and Maxillofacial Radiology (2008) American Academy of Oral and Maxillofacial Radiology executive opinion statement on performing and interpreting diagnostic cone beam computed tomography. *Oral Surg Oral Med Oral Pathol Oral Radiol Endod* 106:561–562. <https://doi.org/10.1016/j.tripleo.2008.07.007>
- Kwong JC, Palomo JM, Landers MA, Figueroa A, Hans MG (2008) Image quality produced by different cone-beam computed tomography settings. *Am J Orthod Dentofacial Orthop* 133:317–327. <https://doi.org/10.1016/j.ajodo.2007.02.053>
- Sur J, Seki K, Koizumi H, Nakajima K, Okano T (2010) Effects of tube current on cone-beam computerized tomography image quality for presurgical implant planning in vitro. *Oral Surg Oral Med Oral Pathol Oral Radiol Endod* 110:e29–e33. <https://doi.org/10.1016/j.tripleo.2010.03.041>
- Dawood A, Brown J, Sauret-Jackson V, Purkayastha S (2012) Optimization of cone beam CT exposure for pre-surgical evaluation of the implant site. *Dentomaxillofac Radiol* 41:70–74. <https://doi.org/10.1259/dmfr/16421849>
- Xi Y, Jin Y, De Man B, Wang G (2016) High-kVp Assisted Metal Artifact Reduction for X-ray Computed Tomography. *IEEE Access* 4:4769–4776. <https://doi.org/10.1109/ACCESS.2016.2602854>
- Bechara B, McMahan CA, Geha H, Noujeim M (2012) Evaluation of a cone beam CT artefact reduction algorithm. *Dentomaxillofac Radiol* 41:422–428. <https://doi.org/10.1259/dmfr/43691321>
- Parsa A, Ibrahim N, Hassan B, Syriopoulos K, van der Stelt P (2014) Assessment of metal artefact reduction around dental titanium implants in cone beam CT. *Dentomaxillofac Radiol* 43: 20140019. <https://doi.org/10.1259/dmfr.20140019>
- Gaêta-Araujo H, Nascimento E, Fontenele RC, Mancini A, Freitas DQ, Oliveira-Santos C (2020) Magnitude of beam-hardening artifacts produced by gutta-percha and metal posts on cone-beam computed tomography with varying tube current. *Imaging Sci Dent* 50: 1–7. <https://doi.org/10.5624/isd.2020.50.1.1>
- Gaêta-Araujo H, Nascimento EHL, Oliveira-Santos N, Pinheiro MCR, Coelho-Silva F, Oliveira-Santos C (2020) Influence of adjacent teeth restored with metal posts in the detection of simulated internal root resorption using CBCT. *Int Endod J* 53:1299–1306. <https://doi.org/10.1111/iej.13348>
- Pauwels R, Seynaeve L, Henriques JC, de Oliveira-Santos C, Souza PC, Westphalen FH, Rubira-Bullen IR, Ribeiro-Rotta RF,

- Rockenbach MI, Haiter-Neto F, Pittayapat P, Bosmans H, Bogaerts R, Jacobs R (2015) Optimization of dental CBCT exposures through mAs reduction. *Dentomaxillofac Radiol* 44:20150108. <https://doi.org/10.1259/dmfr.20150108>
17. Gaêta-Araujo H, Silva de Souza GQ, Freitas DQ, de Oliveira-Santos C (2017) Optimization of Tube Current in Cone-beam Computed Tomography for the Detection of Vertical Root Fractures with Different Intracanal Materials. *J Endod* 43:1668–1673. <https://doi.org/10.1016/j.joen.2017.04.003>
 18. Lopes PA, Santaella GM, Lima C, Vasconcelos KF, Groppo FC (2019) Evaluation of soft tissues simulant materials in cone beam computed tomography. *Dentomaxillofac Radiology* 48:20180072. <https://doi.org/10.1259/dmfr.20180072>
 19. Vasconcelos TV, Leandro Nascimento EH, Bechara BB, Freitas DQ, Noujeim M (2019) Influence of Cone Beam Computed Tomography Settings on Implant Artifact Production: Zirconia and Titanium. *Int J Oral Maxillofac Implants* 34:1114–1120. <https://doi.org/10.11607/jomi.7129>
 20. Freitas DQ, Fontenele RC, Nascimento E, Vasconcelos TV, Noujeim M (2018) Influence of acquisition parameters on the magnitude of cone beam computed tomography artifacts. *Dentomaxillofac Radiol* 47:20180151. <https://doi.org/10.1259/dmfr.20180151>
 21. Fontenele RC, Nascimento EHL, Santaella GM, Freitas DQ (2020) Does the metal artifact reduction algorithm activation mode influence the magnitude of artifacts in CBCT images? *Imaging Sci Dent* 50:23–30. <https://doi.org/10.5624/isd.2020.50.1.23>
 22. Queiroz PM, Oliveira ML, Groppo FC, Haiter-Neto F, Freitas DQ (2018) Evaluation of metal artefact reduction in cone-beam computed tomography images of different dental materials. *Clin Oral Invest* 22:419–423. <https://doi.org/10.1007/s00784-017-2128-9>
 23. Vasconcelos TV, Bechara BB, McMahan CA, Freitas DQ, Noujeim M (2017) Evaluation of artifacts generated by zirconium implants in cone-beam computed tomography images. *Oral Surg Oral Med Oral Pathol Oral Radiol Endod* 123:265–272. <https://doi.org/10.1016/j.o000.2016.10.021>
 24. Omar G, Abdelsalam Z, Hamed W (2016) Quantitative analysis of metallic artifacts caused by dental metallic restorations: comparison between four CBCT scanners. *Future Dent J* 2:15–21. <https://doi.org/10.1016/j.fdj.2016.04.001>
 25. de Azevedo-Vaz SL, Peyneau PD, Ramirez-Sotelo LR, Vasconcelos K, Campos PS, Haiter-Neto F (2016) Efficacy of a cone beam computed tomography metal artifact reduction algorithm for the detection of eri-implant fenestrations and dehiscences. *Oral Surg Oral Med Oral Pathol Oral Radiol Endod* 121:550–556. <https://doi.org/10.1016/j.o000.2016.01.013>
 26. Candemil AP, Salmon B, Freitas DQ, Ambrosano GM, Haiter-Neto F, Oliveira ML (2018) Metallic materials in the exomass impair cone beam CT voxel values. *Dentomaxillofac Radiol* 47:20180011. <https://doi.org/10.1259/dmfr.20180011>
 27. Machado AH, Fardim KAC, Souza CF, Sotto-Maior BS, Assis NMSP, Devito KL (2018) Effect of anatomical region on the formation of metal artefacts produced by dental implants in cone beam computed tomographic images. *Dentomaxillofac Radiol* 47:20170281. <https://doi.org/10.1259/dmfr.20170281>
 28. Queiroz PM, Santaella GM, Paz TDJ, Freitas DQ (2017) Evaluation of a metal artefact reduction tool on different positions of a metal object in the FOV. *Dentomaxillofac Radiol* 46:20160366. <https://doi.org/10.1259/dmfr.20160366>
 29. Pauwels R, Jacobs R, Boegarts R, Bosmans H, Panmekiate S (2016) Reduction of scatter-induced image noise in cone beam computed tomography: effect of field of view size and position. *Oral Surg Oral Med Oral Pathol Oral Radiol* 121:188–195. <https://doi.org/10.1016/j.o000.2015.10.017>
- Publisher's note** Springer Nature remains neutral with regard to jurisdictional claims in published maps and institutional affiliations.